Article

Not peer-reviewed version

Multifunctional Hybrid Material for Endoprosthetic Implants Based on Alumina-Toughened Zirconia Ceramics and Additively Manufactured TiNbTa Alloy

Jan-Oliver Sass *, Paul Henke, Aurica Mitrovic, Markus Weinmann, Daniel Kluess, Jan Johannsen, Marie-Luise Sellin, Ulrich Lembke, Daniel Reimer, Cornelia Lork, Anika Jonitz-Heincke, Rainer Bader

Posted Date: 18 March 2024

doi: 10.20944/preprints202403.0971.v1

Keywords: implant material; hybrid; alumina-toughened zirconia; beta titanium; glass soldering; additive manufacturing; total knee replacement; aseptic loosening

Article

Multifunctional Hybrid Material for Endoprosthetic Implants Based on Alumina-Toughened Zirconia Ceramics and Additively Manufactured TiNbTa Alloy

Jan-Oliver Sass [1,*], Paul Henke [1], Aurica Mitrovic [2], Markus Weinmann [3], Daniel Kluess [1,4], Jan Johannsen [5], Marie-Luise Sellin [1], Ulrich Lembke [6], Daniel Reimer [7], Cornelia Lork [2], Anika Jonitz-Heincke [1] and Rainer Bader [1]

[1] Research Laboratory for Biomechanics and Implant Technology, Department of Orthopaedics, Rostock University Medical Center, Doberaner Straße 142, D-18057 Rostock, Germany
[2] ZM Praezisionsdentaltechnik GmbH, Breite Str. 16, D-18057 Rostock Germany
[3] TANIOBIS GmbH, Im Schleeke 78-91, D-38642 Goslar, Germany
[4] INNOPROFF GmbH, Joachim-Jungius-Straße 9, D-18059 Rostock, Germany
[5] Fraunhofer Research Institution for Additive Manufacturing Technologies IAPT, Am Schleusengraben 14, D-21029 Hamburg, Germany
[6] DOT GmbH, Charles-Darwin-Ring 1A, D-18059 Rostock, Germany
[7] FMZ GmbH, Charles-Darwin-Ring 3A, D-18059 Rostock, Germany
* Correspondence: jan-oliver.sass@med.uni-rostock.de, Tel.: +49 381 494-9338

Abstract: Aseptic implant loosening after total joint replacement is partially influenced by material-specific factors when cobalt-chromium alloys are used, including osteolysis induced by wear- and corrosion products, and stress shielding. Here, we aim to characterize a hybrid material consisting of alumina-toughened zirconia ceramics (ATZ) and additively manufactured Ti-35Nb-6Ta (TiNbTa), joined by a glass solder. The structure of the joint, static and fatigue shear strength, the influence of accelerated aging, and the cytotoxicity using an elution assay with human osteoblasts are characterized. Furthermore, the biomechanical properties of functional demonstrators of a femoral component for total knee replacements are evaluated. TiNbTa-ATZ specimens showed a homogenous joint with statistical distributed micro-pores and a slight accumulation of Al-rich compounds at the glass solder-TiNbTa interface. The static shear strength was 26.4 ± 4.2 MPa (Ti-ATZ reference: 38.2 ± 14.4 MPa, $p = 0.117$), all specimens survived 10^7 cycles of shear loading to 10 MPa, and aging did not reduce the static shear strength. Furthermore, TiNbTa-ATZ did not impair the proliferation and metabolic activity of human osteoblasts. Functional demonstrators made of TiNbTa-ATZ provided a maximum bearable extension-flexion moment of 40.7 ± 2.2 Nm. Biomechanical and biological properties of TiNbTa-ATZ demonstrate potential application for endoprosthetic implants.

Keywords: joint arthroplasty; total knee replacement; implant; aseptic loosening; material joining; alumina-toughened zirconia; beta titanium; glass soldering; additive manufacturing

1. Introduction

Aseptic implant loosening is the main reason for the revision of total joint replacements [1]. Implant material-related complications are associated with wear particles, corrosion products, and the mechanical mismatch of the materials to the human bone [2,3]. Metal wear particles can stimulate osteoclastic bone resorption [2] and released metal ions, e.g. from cobalt-chromium and titanium alloys (Co^{2+}, Cr^{3+}, Al^{3+}, V^{2+}) may cause adverse local [4–6] and systematic biological response [7,8]. Common-used implant materials lead to alteration of mechanical loading of the periprosthetic bone (stress shielding). The mechanical stimulus on the bone tissue and cells is redcued and thus bone

 doi:10.20944/preprints202403.0971.v1

remodeling shifted towards resorption [2,3]. These effects are leading to periprosthetic bone loss, potentially causing osteolysis, implant loosening, and increased periprosthetic fracture risk [9].

Multifunctional hybrid implant materials have been investigated to address these issues [10–18]. For example, these materials are supposed to combine advantageous properties of oxide ceramics at the articulating surfaces of the artificial joint and titanium (Ti) alloys at the bone-implant interface. Thus, high wear and corrosion resistance with a lower risk of stress shielding can be achieved [10,12,14,19]. In previous studies, functionally graded materials manufactured by spark plasma sintering have been investigated [10–14,19]. They are composed of a pure ceramic phase (e. g. Al_2O_3 or Y_2O_3-stabilized ZrO_2), mixed ceramic-titanium phases with continuously decreasing ceramic content, and a titanium or Ti-6Al-4V phase. Other approaches used laser-engineered net shaping to manufacture Ti6Al4V-Al_2O_3 [15] hybrids or glass solders to join solid ceramic and titanium-based components [17,18].

Glass soldering of bioceramics such as Al_2O_3 or ZrO_2 and commercially pure titanium (cp-Ti) has originally been developed for dental applications [20–22] but it also demonstrated applicability to the endoprosthetic implant materials like alumina-toughened zirconia ceramics (ATZ) and Ti-6Al-4V [18]. Processing such hybrid materials involves the application of a biocompatible silica-based glass [18,23] to the joining surfaces and a subsequent firing to melt the glass solder. The main reason for a stable and durable connection is the formation of reaction layers during firing [17,18,24], and the mechanical interlocking between glass solder and ceramic or the metal part, respectively [17]. Mick et al. [18] used a glass solder (main components: SiO_2, Al_2O_3, Na_2O, KO_2) to fabricate Ti6Al4V-ATZ hybrid materials and reported a bending strength of 118 ± 33 MPa. In addition, Markhoff et al. [22] showed good interaction of human osteoblasts with a similar glass solder applied as a coating on ATZ bulk material. Nevertheless, the transformation of this technology to endoprosthetic implants, such as the femoral component of a total knee replacement, presents challenges in joining larger and complex shaped surfaces.

Using medical β-titanium (β-Ti) alloys in glass-soldered hybrid materials is a promising approach, since β-Ti alloys possess increased elasticity compared to pure α (cp-Ti) or α+β (Ti-6Al-4V) Ti alloys [25]. They are mostly composed of biocompatible elements such as Nb, Ta, and Zr [26–28], which are highly corrosion resistant [29,30] and additionally promote osteogenesis [31]. Furthermore, β-Ti alloys can be additively manufactured by laser powder bed fusion (PBF-LB/M) [32], allowing advanced processability, e.g., direct fabrication of complex structures, such as open porous scaffolds or specifically functionalized implant surfaces [26,33]. In this context, Ti-35Nb-6Ta (TiNbTa) additively manufactured by PBF-LB/M has been recently investigated [31,32]. This alloy has a lower elastic modulus of approx. 54.2 GPa [31] compared to commercially-used Ti-6Al-4V (115 GPa [34]). A tensile strength of 651 ± 1.2 MPa and an elongation at break of 21.3 ± 1.2 % was reported, indicating that TiNbTa is also highly ductile [32]. In addition, human osteoblasts cultured on as printed TiNbTa surfaces showed a gene expression profile of osteogenic differentiation markers, indicating osteoconductive properties [31].

The present study aims to characterize hybrid TiNbTa-ATZ specimens using additively manufactured TiNbTa components which are joined to ATZ using a biocompatible silica-based glass solder. The manufactured TiNbTa-ATZ joints are structurally and chemically analyzed by backscatter electron (BSE) microscopy and energy-dispersive X-ray spectroscopy (EDX). Furthermore, the hybrid material is characterized by mechanical testing (static and fatigue shear stress) and the influence of artificially aging on static shear strength is analyzed. Hybrid Ti-ATZ specimens are used as a reference. In addition, the cytotoxicity of TiNbTa-ATZ specimens is evaluated and compared with Ti-ATZ and Co-CrMo specimens using an elution assay and human osteoblasts. Furthermore, a simplified functional implant demonstrator of a hybrid material-based femoral component was fabricated, structurally characterized, and analyzed for mechanical strength under biomechanical loading using gait cycles as well as loading to failure.

 doi:10.20944/preprints202403.0971.v1

2. Materials and Methods

2.1. Manufacturing of The Hybrid Material

Hybrid material specimens made of slip-casted ATZ (Koebel Engineering, Dachsen, Switzerland) and TiNbTa were manufactured and joined applying glass soldering. Hybrid Ti-ATZ materials were used as reference. The TiNbTa components were additively manufactured using PBF-LB/M. The spherical TiNbTa powder was produced by electrode induction melting gas atomization (EIGA), which was conducted under purified argon (4.6, Linde GmbH, Pullach, Germany) atmosphere from pre-alloyed electrodes (TANIOBIS GmbH, Goslar, Germany) [32]. In a previous study with similar powder, the measured chemical composition, determined by inductively coupled plasma optical emission spectroscopy (ICP-OES) was 58.87 wt. % Ti, 34.45 wt. % Nb, and 5.98 wt. % Ta [32]. PBF-LB/M was done using a DMP350 Flex (3D Systems Corp., Rock Hill, SC, USA) equipped with a 1 kW single-mode laser (YLR-1000-WC-Y14, IPG Laser GmbH, Burbach, Germany) under argon gas atmosphere to prevent oxidation. The scanning speed was 1500 $mm \times s^{-1}$, the laser power was 170 W, the layer thickness was 0.3 mm, and the hatch distance was 69 µm. Similar powder, devices, and process parameters led to dense parts with a homogenous element distribution and a monocrystalline β-phase [32]. After additive manufacturing, the end faces of the cylindrical TiNbTa specimens used for shear testing were machined to meet the parallelism requirements of the joining surfaces.

The main components of the silica-based glass solder (DCMhotbond fusio-12, DCM Dental Creative Management GmbH, Rostock, Germany) were SiO_2 (63 - 67 wt. %), Al_2O_3 (6 - 9 wt. %), K_2O (6 – 9 wt. %), and Na_2O (6 - 9 wt. %). The glass solder had a coefficient of thermal expansion (CTE) of 10.0×10^{-6} K^{-1}, a melting temperature of 450 °C, and a bending strength at room temperature of ≥ 50 MP (provided by ZM Praezisionsdentaltechnik GmbH, Rostock, Germany). The ATZ ceramics had a CTE of $7.8 – 8.1 \times 10^{-6}$ K^{-1}(provided by Koebel Engineering, Dachsen, Switzerland). Further, the CTE of Ti-35Nb-6Ta is temperature-dependent and ranged, in the relevant temperature regime of 20°C to 450°C (melting point of the glass solder) from 8.2×10^{-6} K^{-1} to 9.3×10^{-6} K^{-1} (provided by TANIOBIS GmbH, Goslar, Germany). Similar to previous studies [18,23], the soldering was performed in a furnace and according to the guidelines provided by DCM Dental Creative Management GmbH, Rostock, Germany. Before glass soldering, the joining surfaces were sandblasted (110 µm Al_2O_3 at 4 bar), cleaned in an ultrasonic bath in ethanol, and then primed with a thin layer of the glass solder. After sandblasting, TiNbTa and cp-Ti components had an average roughness of 1.5 ± 0.1 µm and 1.7 ± 0.1 µm, respectively (measured using the laser scanning microscope VK-X250, Keyence Corporation, Osaka, Japan). Finally, a glass solder paste was applied to the joining surfaces and fired at 820°C for 5 min, using a heating and cooling rate of 20 $K \times min^{-1}$. The joined interface of the TiNbTa-ATZ specimens was analyzed by BSE and EDX using an SEM JSM6490 (Jeol, Akishima, Tokyo, Japan) equipped with an X-Flash SEM 4010 (Bruker Nano GmbH, Berlin, Germany) for structural and chemical analysis.

2.2. Shear Testing, Artificial Aging, and Fracture Analysis

The static and dynamic shear testing of the hybrid materials was performed according to relevant standards [35–37]. Furthermore, the influence of artificial aging (0.5 MPa, 70 °C, 14 days [38]) on static shear strength was evaluated. Accordingly, six different groups (Table 1) were characterized, and each group contained n = 5 specimens.

Table 1. Overview of the mechanically tested groups, the used hybrid material, test specifications, and the measured cross-section at the soldered joint.

Group	Material	Specifications	Cross-section [mm^2]
1	TiNbTa-ATZ	Static shear test	279.4 ± 0.1
2	Ti-ATZ	Static shear test	280.0 ± 0.3
3	TiNbTa-ATZ	Accelerated aging followed by static shear test	281.0 ± 1.1

 doi:10.20944/preprints202403.0971.v1

4	Ti-ATZ	Accelerated aging followed by static shear test	280.4 ± 0.4
5	TiNbTa-ATZ	Fatigue shear test	280.3 ± 0.8
6	Ti-ATZ	Fatigue shear test	281.9 ± 1.2

The static shear tests were conducted using a universal testing machine (Zwick 50kN RetroLine, Zwick Roell, Ulm, Germany). The specimens were loaded until fracture at a rate of 2.5 mm×min^{-1}. The fatigue tests were performed using an electro-dynamic testing machine (ElectroForce 3510, TA Instruments – Waters LLC, Eden Prairie, MN, USA) with a sinusoidal load between 1 MPa and 10 MPa, and frequency of 10 Hz [39]. 10^7 cycles were defined as a successful test [35].

After mechanical testing, the fractured surfaces of all specimens were analyzed with a digital microscope (VHX-6000) and laser scanning microscope (VK-X250, both: Keyence Corporation, Osaka, Japan) to determine causes of fracture.

2.3. Biological Characterization

For the biological characterization of the hybrid material specimens (TiNbTa-ATZ and Ti-ATZ), cytotoxicity measurements were performed by an elution assay and commercially-used Co-28Cr-6Mo specimens served as a negative control. The specimens had a diameter of 12 mm and were 5 mm in height. The heat sterilized specimens were first covered with 838 µl of calcium-free Dulbecco's Modified Eagle's Medium (DMEM) per sample and incubated at 37 °C and 5 % CO_2 for 14 and 21 days. A medium control without samples was included.

For the cytotoxicity assays, human osteoblasts were isolated from the femoral heads of patients undergoing total hip arthroplasty according to an established protocol by Lochner et al. [40]. Femoral heads were provided after informed consent was obtained from the patients. The study was approved by the ethics committee of the University Medical Center Rostock (A 2010-0010). Experiments were performed with human osteoblasts from eight donors (n = 8, female: n = 4, mean age: 61 ± 7.3 years; male: n = 4, mean age: 57 ± 4.5 years). Cells were cultured under standard culture conditions at 37 °C and 5 % CO_2 in calcium-free DMEM supplemented with 10 % fetal calf serum (FCS; both: PAN-Biotech, Aidenbach, Germany), 1 % amphotericin B, 1 % penicillin-streptomycin, and 1 % HEPES buffer (all: Sigma-Aldrich, Munich, Germany). To maintain the osteogenic phenotype, 10 mM β-glycerophosphate, 50 µg×ml^{-1} ascorbic acid, and 100 nM dexamethasone were added to the cell culture medium (all: Sigma-Aldrich, Munich, Germany). 10000 osteoblasts per well were seeded in a 96-well plate (Thermo Fisher Scientific Inc., Waltham, MA, USA) and incubated for 24 hours, followed by incubation with the material eluates. For this purpose, the respective eluates were diluted 1:1 with fresh medium containing osteogenic additives. Osteoblasts were incubated with 150 µl of the diluted eluate for 24 hours. The viability of osteoblasts after incubation was evaluated via the metabolic activity assay water-soluble tetrazolium salt (WST-1; Takara Bio, Saint-Germain-en-Laye, France) and CyQUANT™ NF Cell Proliferation Assay (ThermoFisher Scientific, Waltham, MA, USA). First, the metabolic activity was determined. The medium was removed, and the cells were washed with PBS. The cells were then incubated with a defined volume of WST-1/medium reagent (1:10 ratio) at 37 °C and 5 % CO_2. After an incubation period of 30 min, 100 µl of the supernatants were transferred to a 96-well cell culture plate, and the absorbance at 450 nm (reference wavelength: 630 nm) was measured in a microplate reader (Tecan Reader Infinite® 200 Pro, Tecan Trading AG, Maennedorf, Switzerland). To determine the absolute cell number, the CyQUANT™ Cell Proliferation Assay was performed according to the manufacturer's guideline. The same cells for which the metabolic activity was previously determined were used. They were covered with 100 µl of 1x Dye Binding Solution (consisting of 1:500 Dye Reagent and 1x HBSS) and incubated at 37 °C, protected from light. After 60 min, the fluorescence intensity was measured at 530 nm (excitation wavelength: 485 nm) using the Tecan Infinite® 200 Pro reader. A cell number calibration curve was generated using pre-defined cell numbers in duplicate to relate the fluorescence signal to the actual cell number.

 doi:10.20944/preprints202403.0971.v1

2.4. Biomechanical Characterization of Functional Demonstrators

2.4.1. Demonstrator Manufacturing

Based on the geometries of commercially available total knee endoprostheses [41], a simplified functional demonstrator was designed in Creo Parametrics 10.0.0.0 (PTC, Boston, MA, USA) to gain experience with more complex shaped soldering components. The simplification was necessary to to achieve the next development step. The functional demonstrator represented one condyle of the tibiofemoral joint (Figure 1) with an outer radius of 30 mm and a depth of 22.5 mm. Since a homogeneous joint gap is crucial for the glass soldering process, a frame and spacers were designed on the titanium component with 0.1 mm in height. The titanium-based component was further designed to enable clamping of the functional demonstrator during the biomechanical testing and geometric cutouts were designed to reduce the amount of heat absorption during the firing process.

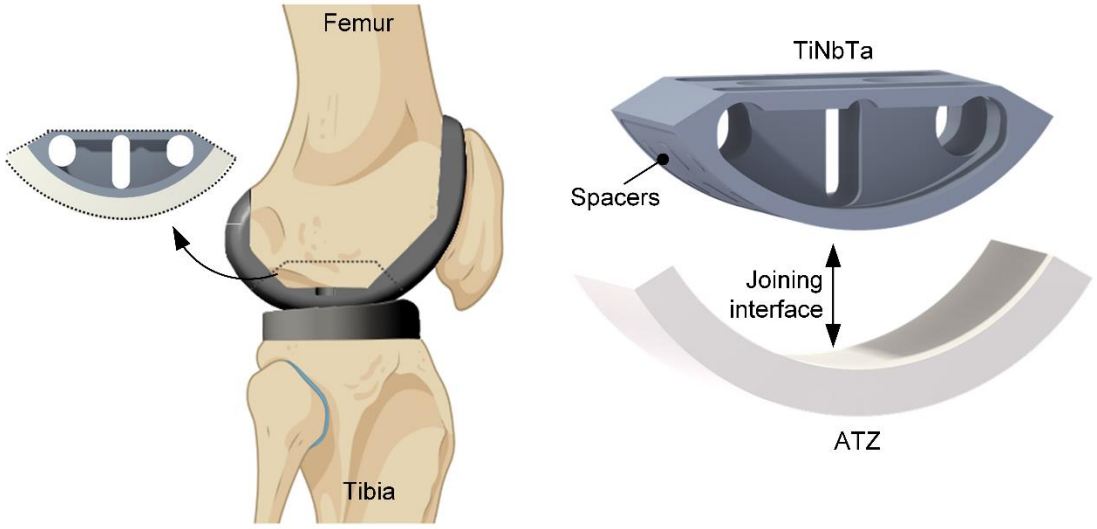

Figure 1. Design of the simplified functional demonstrator of a hybrid material-based femoral component for a total knee replacement resembling a part of the tibiofemoral joint. The hybrid material is formed by glass soldering of additivly manufactured TiNbTa to ATZ ceramics and the joining surface of TiNBTa is functionalized with spacers 0.1 mm in height to ensure a homogeneous joint gap (created with Biorender.com).

For glass soldering, the joint surfaces were sandblasted (110 µm Al_2O_3 at 4 bar) and cleaned with ethanol in an ultrasonic bath for 3 min. The average roughness values (measured by laser scanning microscopy) of the sandblasted TiNbTa (PBF-LB/M) and cp-Ti (CNC machined) components were 5.8 ± 2.0 µm and 1.9 ± 0.3 µm, respectively. In general, the soldering followed the same procedure as described in section 2.1, but a more extensive priming of the surfaces was conducted to omit pore formation in the soldered joint. The first priming was done by spray-coating with the glass solder paste. A firing process of the individual parts was conducted subsequently to establish the joint between the glass solder and ATZ and and the titanium-based material, respectively. After the first priming of the titanium-based component, the soldering surface was polished (600 µm and 1000 µm grit), covered with glass solder paste, and fired again. This process was repeated two times to fill the room between the spacers with the glass solder. In Figure 2, the initial additively manufactured TiNbTa component along with the spray-coated specimen and the final stage of priming are illustrated.

 doi:10.20944/preprints202403.0971.v1

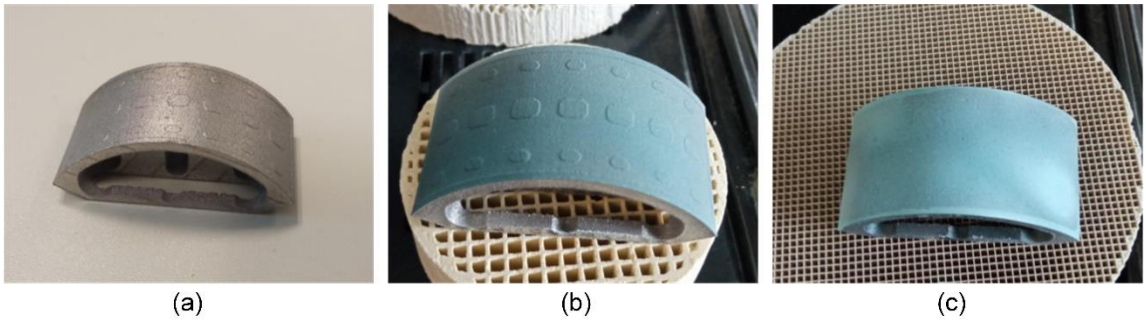

Figure 2. Consecutive steps to prime the TiNbTa component of the hybrid material-based functional demonstrator with a) untreated specimen, b) specimen coated with the glass solder, and c) completely primed specimen by stepwise firing and polishing of the glass solder to fill the gap between the designed spacers with the glass solder. For better visualization, the glass solder was dyed blue.

The soldering of the ATZ and the TiNbTa or cp-Ti component was done at 820°C for 5 min. The structure quality of the joint interface was anaylsed by electron microscopy of a polished cross-section of the hybrid TiNbTa-ATZ specimen.

2.4.2. Biomechanical Characterization

The biomechanical characterization of the functional demonstrators comprised two consecutive tests. First, the specimens were loaded for 10000 walking cycles and second, the same specimens were used to evaluate the maximum extension-flexion moment. Each group of either TiNbTa-ATZ or Ti-ATZ hybrids contained n = 3 specimens.

The 10000 walking cycles were applied using a 6-degree-of-freedom joint simulator (VIVO™, Advanced Mechanical Technology, Watertown, MA, USA) according to ISO standard 14243-3:2014 [37]. Therefore, extension-flexion, internal-external rotation, and anterior-posterior translation were position-controlled, and the superior-inferior direction was force-controlled (axial force). The abduction-adduction rotation and medial-lateral translation remained unloaded. The functional demonstrators articulated with ultra-high-molecular-weight polyethylene cylindrical specimens with a flat surface. Silicone oil (Typ 350, Caesar & Loretz GmbH, Hilden, Germany) served as a lubricant. The test setup and applied rheonomic constraints are shown in Figure 3a. Moreover, specimens that survived the dynamic loading were rotationally loaded until failure with $0.1°\times s^{-1}$ (Figure 3b), simulating an extension-flexion moment. The ATZ component was constrained in the yz-plane (sagittal plane) and the moment was applied through the titanium component and the rotational center of the functional demonstrator.

 doi:10.20944/preprints202403.0971.v1

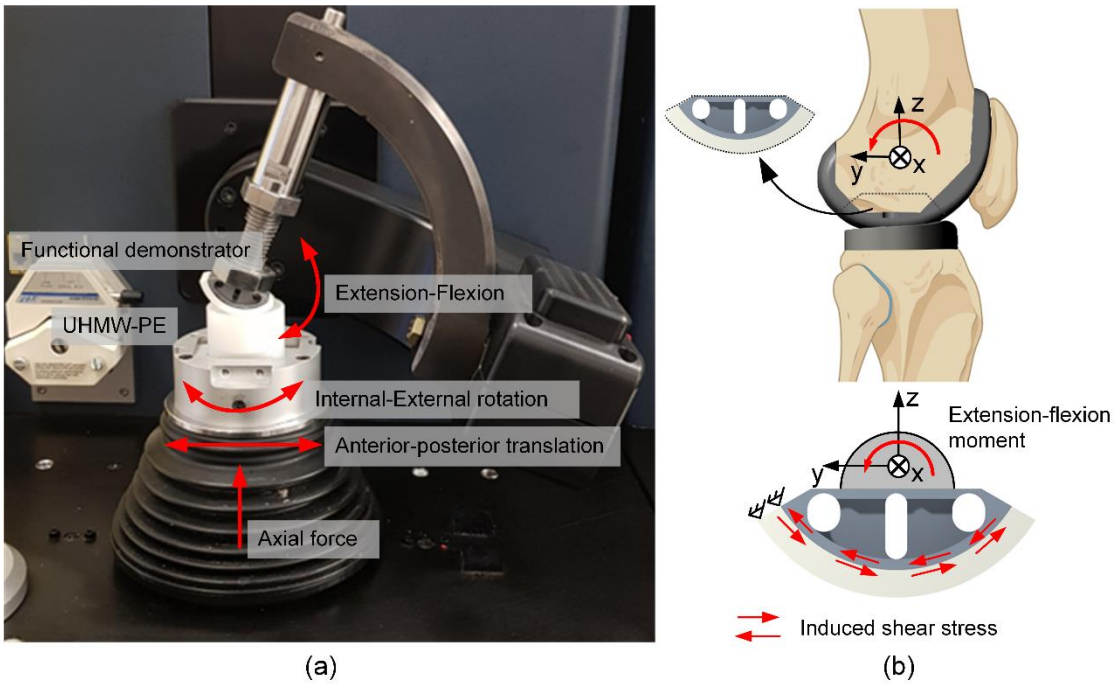

Figure 3. Biomechanical characterization of the hybrid material-based (glass soldered TiNbTa-ATZ or Ti-ATZ) functional demonstrators of the femoral component of a total knee replacement: a) biomechanical loading of the walking cycle in the VIVO™ joint simulator and b) schematic illustration of the flexion movement of the tibiofemoral joint and derived test setup to characterize the maximum bearable extension-flexion moment (created with Biorender.com).

2.5. Statistical Analysis

Statistical analysis of the results was performed in GraphPad Prism 9.2 (GraphPad Software, San Diego, CA, USA) and $p < 0.05$ was used as the level of significance. The results of the shear testing were checked for significant differences by the Kruskal-Wallis-Test. For the cytotoxicity tests, comparisons between experimental groups were performed using 2-way ANOVA and Bonferroni Multiple Comparison Test. All data are presented as individual values with median and interquartile ranges.

3. Results

3.1. Structurual, Local Chemical and Mechanical Characterisation

The structural and local chemical analysis by electron microscopy of a polished cross-section of a TiNbTa-ATZ specimen is shown in Figure 4. The BSE image in Figure 4a points to the fact that the soldering occurred very homogeneously. The thickness of the solder was slightly below 100 µm. Occasionally, spherical pores were visible in the solder, with diameters in the single digit micro region, as evident from the magnified spot displayed in Figure 4d. The elemental mapping of the TiNbTa component (Figure 4b) displayed a homogenous element distribution of the constituting elements. In contrast to the as-atomized TiNbTa powder, no segregation into Ti or Nb/Ta enriched dendrite type structures was observed. ATZ (Figure 4c) represents a two-phase material in which sub-micron Al_2O_3 particles were evenly embedded in a ZrO_2 matrix. The element mapping of the solder displayed in Figure 4e reveals a local accumulation of Al at the glass solder-TiNbTa interface. Besides these features the glass solder was constituted by a homogenous SiO_2, K_2O, Na_2O matrix containing Al_2O_3 segregations (Figure 4f).

 doi:10.20944/preprints202403.0971.v1

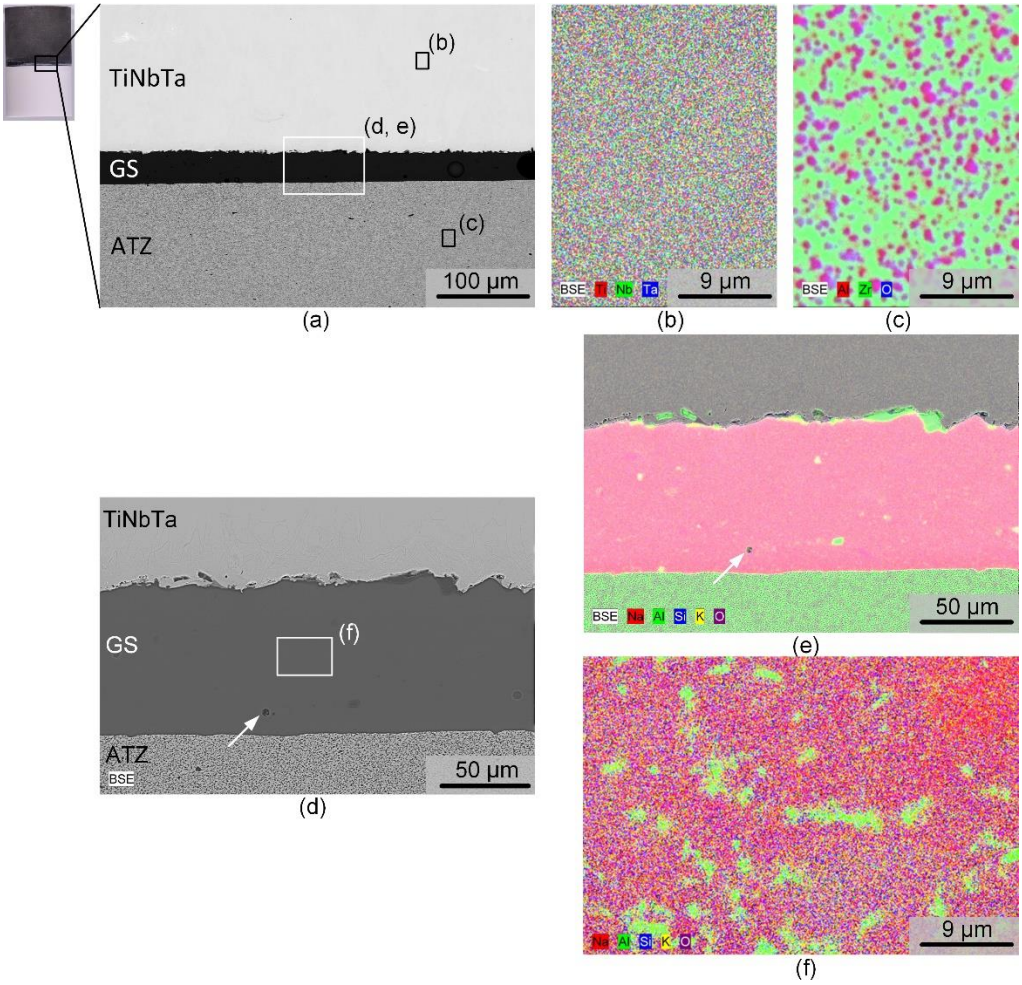

Figure 4. Electron microscopic images of a hybrid material of joined alumina-toughened zirconia (ATZ) and additively manufactured Ti-35Nb-6Ta (TiNbTa) using a silica-based glass solder (GS). a,d) BSE of the investigated cross-section, at different magnifications, b,c,e,f) element distribution in the TiNbTa alloy (b), the ATZ ceramic (c), and the glass solder (e, f). Pores are indicated by white arrows.

The results of the static shear tests are shown in Figure 5a. The static shear strength of TiNbTa-ATZ and Ti-ATZ specimens (group 1 vs. group 2) was 26.4 ± 4.2 MPa and 38.2 ± 14.4 MPa ($p = 0.117$), respectively. The static shear strength of artificially aged TiNbTa-ATZ and Ti-ATZ specimens (group 3 vs. group 4) was 32.1 ± 1.4 MPa and 44.1 ± 9.7 MPa ($p = 0.075$), respectively. Aged TiNbTa-ATZ specimens showed significantly higher shear strength compared with non-aged TiNbTa-ATZ specimens ($p = 0.016$). Both hybrid materials (groups 5 and 6) survived 10^7 cycles at 10 MPa dynamic shear loading without fracture

A mixed mode of failure in the Ti-based bulk material (cohesive failure) and failure in the glass solder (adhesive failure) was observed in different proportions (Figure 5b). Cohesive failure was visible as deposition of the material on the ATZ component, as can be seen by the depth profile in Figure 5e. Furthermore, it was observed that specimens with predominantly cohesive failure had higher shear strengths compared to specimens that mainly fractured in the glass solder (Figure 5b). Pore formation locally hindered the bonding of the materials, causing imperfections in the soldered joint. These imperfections were randomly distributed across the surfaces and were either spherical (Figure 5f-h) or formed a networked or branched structure (Figure 5i-k).

 doi:10.20944/preprints202403.0971.v1

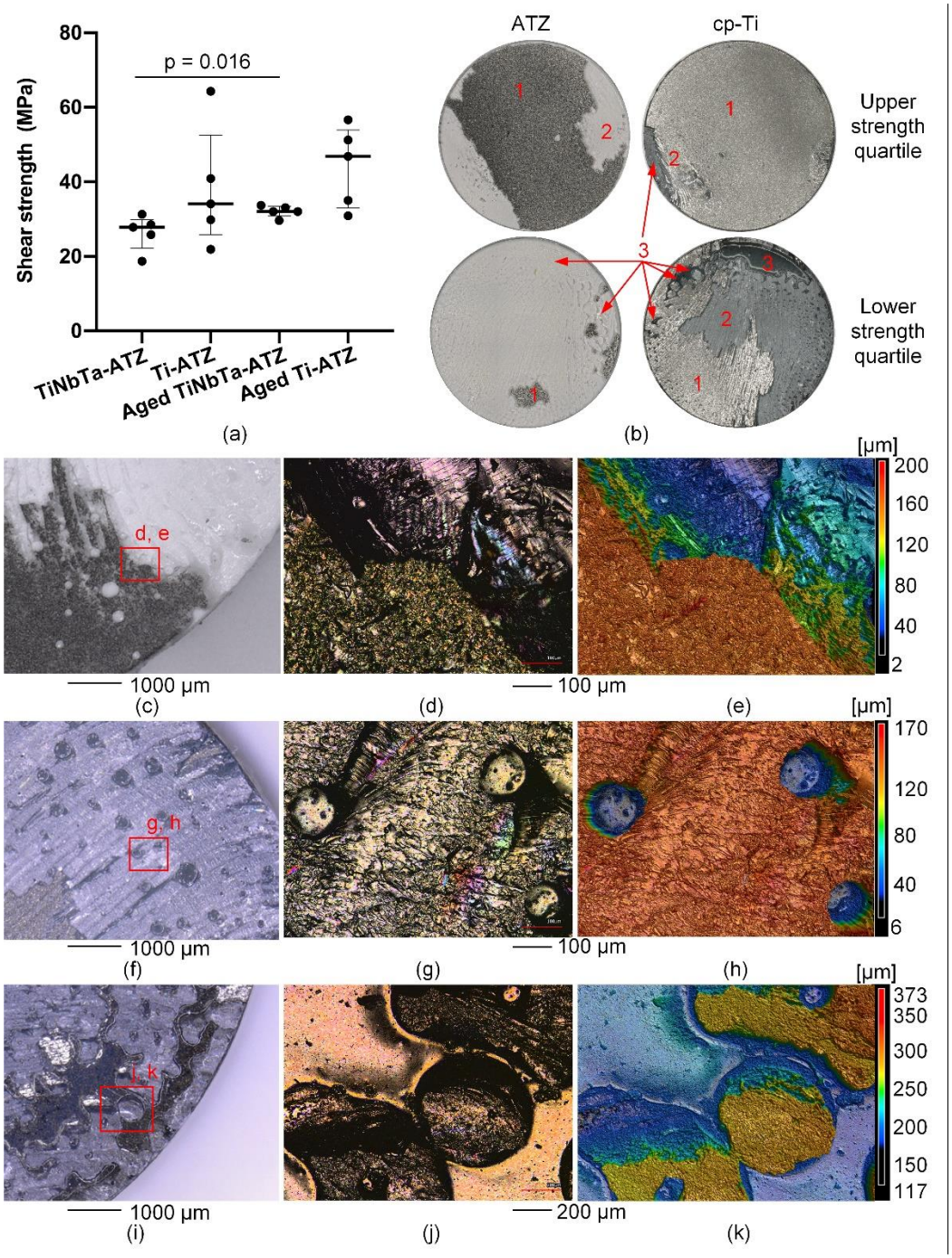

Figure 5. Results of the static shear testing and microscopy of the fracture surfaces of glass-soldered TiNbTa-ATZ or Ti-ATZ hybrids. a) static shear strength (data are presented as single values with median and interquartile ranges and statistical significance was determined by a pairwise Kruskal Wallis Test), b) representative fracture surfaces of specimens in the upper and lower quartile of the static strength (1: cohesive failure of the Ti-based component, 2: adhesive failure of the glass solder, 3: imperfections in the glass solder due to spherical pores), c-e) Microscopic images and a depth profile of an ATZ fracture surface of a Ti-ATZ specimen indicating the cohesive failure of the cp-Ti, which led to the deposition of the bulk material on the ATZ surface, d-h) Microscopic images and a depth profile of a TiNbTa fracture surface of a specimen of group 1 indicating spherical pores in the glass solder, i-k) Microscopic images and a depth profile of an cp-Ti fracture surface of a specimen of group 4 indicating networked or branched structures in the glass solder.

 doi:10.20944/preprints202403.0971.v1

3.2. Biological Characterization

The eluates from the hybrid material specimens did not affect the proliferation of human osteoblasts (Figure 6a). No difference could be detected between the medium controls (dashed line) or between the incubation times of the eluates. However, cells exposed to the Co-28Cr-6Mo alloy eluates after 14 days showed a tendency to reduce cell proliferation. The day 21 eluates had no effect compared to the medium control and the hybrid material specimens. In contrast to proliferation, the metabolic activity of human osteoblasts was clearly but not significantly reduced by the 21-day Co-28Cr-6Mo alloy eluates (Figure 6b). In contrast, the eluates from the hybrid material specimens did not affect metabolic activity. Incubation of cells with eluates of TiNbTa-ATZ specimens resulted in significantly higher metabolic activity compared to eluates of Co-28Cr-6Mo ($p = 0.008$).

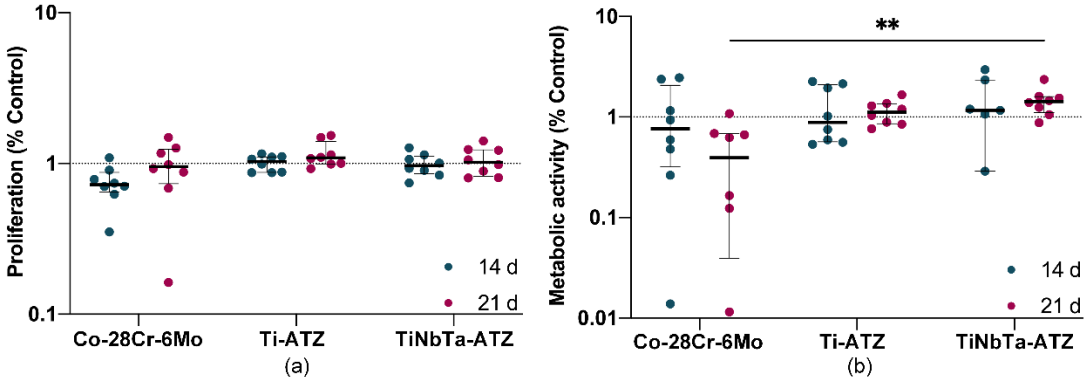

Figure 6. Cytotoxicity analysis of the glass-soldered hybrid material specimens (TiNbTa-ATZ or Ti-ATZ) using elution testing (elution time 14 and 21 days). Quantification of a) metabolic activity by WST-1 assay and b) cell number by CyQUANT™ assay of human osteoblasts after incubation in diluted eluate for 24 h. Osteoblasts in cell culture medium served as control (dashed line). Data are presented as single values with median and interquartile ranges. Statistical significance was determined by 2-way ANOVA followed by Bonferroni multiple comparison test **$p<0.01$.

3.3. Biomechanical Characterization of the Demonstrator

Structural analysis of the soldered joint of a TiNbTa-ATZ functional demonstrator revealed a homogenous joint gap and pores within the glass solder (Figure 7), as already observed for the soldered cylindric specimens (Figure 4). Due to the high quality of the bond, all specimens survived a fatigue test with 10000 simulated gait cycles. The maximum extension-flexion moments were 40.7 ± 2.2 Nm (individual values: 42.2 Nm, 42.3 Nm, 37.7 Nm) and 18.4 ± 3.8 Nm (individual values: 17.2 Nm, 14.5 Nm, 23.5 Nm) of functional demonstrators consisting of TiNbTa-ATZ and Ti-ATZ, respectively. In accordance to the shear-induced fracture, all specimens showed a mixed cohesive and adhesive failure.

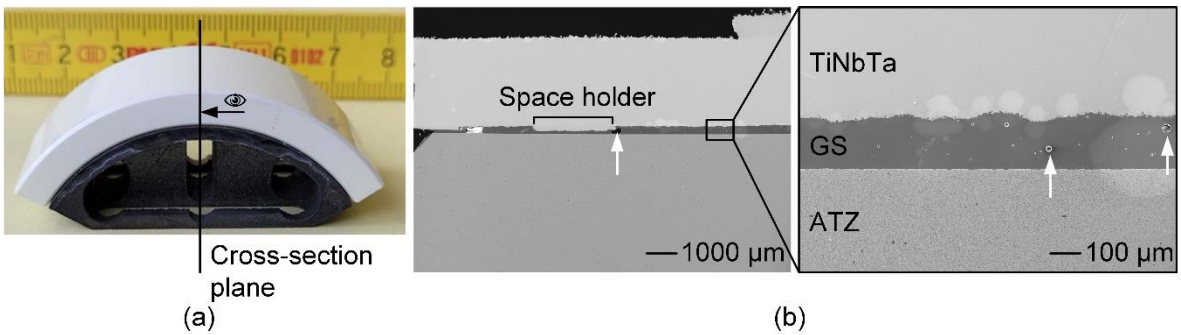

Figure 7. Structural analysis of the functional demonstrator of the femoral component of a total knee replacement made of alumina-toughened zirconia (ATZ) and additively manufactured Ti-35Nb-6Ta (TiNbTa), joined by a silica-based glass solder (GS): a) illustration of the analysed cross-section, b)

 doi:10.20944/preprints202403.0971.v1

BSE of the polished cross-section of the soldered joint; examples of pores in the glass solder are highlighted by white arrows.

4. Discussion

Multifunctional hybrid materials have been described to reduce material-related aseptic implant loosening in total joint replacements [10–18]. These hybrid materials are composed of an oxide ceramic at the articulating interfaces and a Ti-based material at the bone-implant interface. One feasible technology to combine oxide ceramics with Ti alloys is glass soldering [17,18,20,21]. Here, we investigated the static and fatigue shear strength, influence of aging, and cytotoxicity of hybrid material specimens consisting of slip-casted ATZ and additively manufactured β-type Ti-35Nb-6Ta joined by a silica-based glass solder. In addition, the biomechanical performance of functional demonstrators of a total knee replacement was analyzed under walking cycles and load-to-failure testing under an extension-flexion loading.

The static shear strength of TiNbTa-ATZ hybrid material (26.4 ± 4.2 MPa) did not differ significantly compared to the reference material (Ti-ATZ) and showed sufficient fatigue strength to withstand 10^7 dynamic shear loading cycles. Furthermore, accelerated aging caused no reduction in the static shear strength of the joined TiNbTa-ATZ specimens. A comparable study investigating Ti-ZrO_2 hybrid materials reported a shear strength of 16.8 ± 4.9 MPa [24].

To be used as implant material in cementless total joint replacements, the soldered joint of the hybrid material should not represent a predetermined fracture point. In the case of cementless fixated titanium-based implants, the fixation strength between the bone and the implant surface determines the maximum load-bearing capacity. It has been reported that the implant-bone interface strength ranged from 0.5 MPa to 19.7 MPa [42–46]. In addition, in the standard to evaluate the shear strength of titanium-based plasma-sprayed coatings, 20 MPa has been defined as minimum requirement [39]. Therefore, according to the measured properties, the investigated hybrid materials have sufficient strength to ensure that they do not form a flaw when used in endoprosthetic implants. However, during functional loading, the hybrid material is subjected to mixed tensile, shear, and compressive stress [47]. Investigating the influence of the different stresses occurring simultaneously is complex and requires further studies that go beyond the content of the present study.

The microscopic investigations of the TiNbTa-ATZ fracture surfaces revealed that the strength of the hybrid material is determined by adhesive failure along the interface between glass solder and TiNbTa alloy as well as cohesive fracture of the glass solder, which is in line with previous observations [18,20,24]. Within TiNbTa alloys, oxide films, e.g., TiO_2, Nb_2O_5, and Ta_2O are formed [29,30], and the reaction of the chemical compounds in the surface layers with the glass solder is crucial in the formation of the material bond [17,18]. Hey et al. [48] described the formation of Ti_5Si_3 due to the reaction of SiO_2 with Ti using a comparable silica-based glass solder. Furthermore, in a study on the diffusion bonding of Al_2O_3 and cp-Ti, Travessa et al. [49] described that at 800 °C Al_2O_3 dissolves in the presence of titanium and further reacts with titanium to form an intermetallic Ti_3Al compound. In the process, oxygen diffuses into titanium, and Al-rich compounds accumulate at the interface, which was also observed in our study. In contrast, no chemical reaction of Ti-30Ta and Ti-40Nb with Al_2O_3 has been reported [50,51], and also no measurable formation of an interfacial reaction phase of pure Nb with Al_2O_3 [52]. Therefore, it seems reasonable that the material bond between glass solder and TiNbTa was formed by the reaction of titanium with SiO_2 and Al_2O_3. Moreover, it has been previously described that the formed oxide layer in the titanium material or the interface between the oxide layer and the bulk material was responsible for the failure of interfaces between titanium and glass ceramics [18,20]. This was also shown in our present study by the visible deposition of the TiNbTa or cp-Ti on the ATZ fracture surface. The described chemical reactions should be verified in future research focusing on the formation of the intermetallic reaction zone.

Transferring the knowledge gained from glass soldering to more complex and larger joining surfaces is crucial for the development of a hybrid material-based endoprosthetic implant. To gain first experience of the feasibility, we manufactured a simplified functional demonstrator resembling

 doi:10.20944/preprints202403.0971.v1

one condyle of the tibiofemoral joint. As we already observed pores in the soldered joints of the shear test specimens, we tried to reduce them by modifying the priming of the joining surfaces. To achieve a constant joint thickness, the titanium components were provided with spacers. Despite these efforts, pores were still visible in the joint gaps. Nevertheless, all specimens survived 10000 walking cycles and TiNbTa-ATZ hybrids showed maximum extension-flexion moments of 40.7 ± 2.2 Nm. The rather small standard deviations indicate that the modification of the priming processes had a positive influence on variations in the mechanical properties.

Given the absence of prior experiences with the investigated hybrid material regarding biomechanical loading scenarios, the walking cycles gave a first impression of the biomechanical performance of the implant demonstrator. We admit that 10000 cycles are not enough to prove fatigue strength under physiological loading. For example, the ISO standard 14243 specifies 5×10^6 load cycles corresponding to approximately five years of clinical use. In addition to the walking cycles, subsequent loading to failure was used to determine the maximum extension-flexion moment. Bergmann et al. [53] reported data of instrumented TKR and defined the EXTREME100 case as the maximum value suitable for studying mechanical safety under severe *in vivo* conditions. The flexion moments during walking and jogging were 25.9 Nm and 39.8 Nm, respectively, and significantly higher values of 46.1 Nm and 59.1 Nm have been observed during squatting and stair descent, respectively [53]. Another study by Dreyer et al. [54] determined peak values during various physiological motions in a comparable range (26 to 35 Nm). Considering that the maximum extension-flexion moment of the functional demonstrator was observed for a single condyle and that *in vivo* loads are measured for a bicondylar TKR, it seems that the bonding strength of the TiNbTa-ATZ hybrid meets the minimum requirement for an endoprosthetic implant. However, as mentioned above, the total knee endoprostheses are subjected to complex loadings by superimposed forces and moments. In addition, the material joint strength should provide a high safety factor that ensures mechanical functionality over a long period. The bonding strength of complex-shaped hybrid material specimens should therefore be improved, e.g., by realizing a form fit of the ATZ and titanium components.

We observed a difference in the maximum extension-flexion moments of TiNbTa-ATZ and Ti-ATZ functional demonstrators, although no significant differences were observed during shear loading tests. For shear loading, the additive manufactured TiNbTa was machined to obtain parallel joining surfaces and afterward sandblasted (see section 2.2). This procedure led to similar roughness of the different specimens. However, the joining surfaces of the TiNbTa components of the functional demonstrator were not machined, and only sandblasting of the as-printed surface with similar process parameters to cp-Ti components was used. For this reason, the TiNbTa components possessed a higher roughness than those of cp-Ti. In addition to the chemical bond, mechanical interlocking can also majorly contribute to bonding strength [17], that may have led to the increased joint strength in the rougher TiNbTa demonstrators. However, no study investigated the influence of the surface roughness of additively manufactured TiNbTa components on the bonding strength with a silica-based glass solder so far. Therefore, this might be one factor to further increase bonding strength.

In addition to the mechanical properties, the cytotoxicity of the hybrid materials specimens is relevant for later application as bone implants. In our present study, TiNbTa-ATZ specimens did not impair the vitality of human osteoblasts, whereas Co-28Cr-6Mo decreased cell proliferation and metabolic activity. The cytotoxic effect of released Co- and Cr-ions on human cells has been previously demonstrated in various studies [4–8]. In contrast to CoCrMo alloy, the materials based on glass solder and oxide ceramics are highly biocompatible [22]. In addition, it has been shown that osteoblasts cultured on TiNbTa exhibit a gene differentiation indicating bone formation [31]. In line with these previous findings, we demonstrated that the hybrid TiNbTa-ATZ material showed no cytotoxic effects *in vitro*.

However, this study has some limitations. We observed pores in the soldered interface that reduce the mechanically loaded cross-section area. Such faults may cause local stress concentrations resulting in unexpected failure. The pores are based on entrapped gas, which might come from the

 doi:10.20944/preprints202403.0971.v1

evaporation of the polymer-based carrier suspension of the glass solder paste during firing. Minimizing the pore formation is a critical issue to manufacture reliable bonding with glass solders [23,55]. The development of technological approaches to prevent these pores was beyond the scope of this present study. In addition, the functional demonstrator represents a simplified implant design. Hence, the observations during biomechanical testing need to be verified with a more complex design, which is closer to the currently used implants.

Further research should focus on parameter characterization for the bonding strength of TiNbTa-ATZ hybrid materials, e.g., by characterizing the influence of the surface roughness or the chemical composition of the glass solder and joining parameters.

4. Conclusion

TiNbTa-ATZ hybrids combine high wear and corrosion resistance of ATZ ceramics and enhanced osseoconductivity of TiNbTa alloys. The characterized hybrid materials showed good mechanical strength for later use as bone implants. In line with the intrinsic properties of the specific materials, the TiNbTa-ATZ hybrid material showed no cytotoxic effect on human osteoblasts. Therefore, our data indicate the potential of hybrid TiNbTa-ATZ implant material for the use in joint endoprostheses.

Author Contributions: Conceptualization, J.-O. S., A. M., M. W., D. K., J. J., U. L., D. R., C. L., A. J.-H., and R. B.; methodology, J.-O. S., P. H., A. M., M. W., D. K., M.-L. S., U. L., D. R., C. L., A. J.-H., and R. B.; formal analysis, J.-O. S., M.-L. S., and A. J.-H.; investigation, J.-O. S., P. H., M.-L. S., D. K., M. W., A. J.-H., and R. B.; data curation, J.-O. S., P. H. M.-L. S., A. J.-H., and M. W.; writing—original draft preparation, J.-O. S., M.-L. S., and A. J.-H.; writing—review and editing, P. H., A. M., M. W., D. K., J. J., U. L., D. R., C. L., and R. B.; visualization, J.-O. S., M.-L. S., and A. J.-H.; supervision, D. K., A. J.-H., and R. B.; project administration, J.-O. S., and C. L.; funding acquisition, A. M., M. W., D. K., J. J., D. R., U. L., C. L., A. J.-H., and R. B. All authors have read and agreed to the published version of the manuscript.

Funding: This research study was supported by the German Federal Ministry of Education and Research (BMBF, grant number: 03XP0279D), which had no role in study design; in the collection, analysis, and interpretation of data; in the writing of the report; and in the decision to submit the article for publication. The authors also gratefully thank the German Research Foundation (DFG) for funding the VIVO™ joint simulator (GZ: INST 2268/17-1 FUGG), and the European Union and the state of Mecklenburg-West Pomerania (Germany) for funding the laser scanning microscope (VK-X250, grant number GHS-15-0016) and digital microscope (VHX-6000, grant number GHS-16-0002).

Institutional Review Board Statement: The biological characterization using human osteoblasts was conducted in accordance with the Declaration of Helsinki, and approved by the Institutional Review Board (or Ethics Committee) of the University Medical Center Rostock (A 2010-0010).

Data Availability Statement: The data presented in this study are available on request from the corresponding author.

Acknowledgments: We would like to thank Dr. Christian Kaddick and Thuy Linh Le (both: Endolab GmbH, Riedering, Germany) for performing the artificial aging, Dr. Danny Vogel and Mario Jackszis (both: Research Laboratory for Biomechanics and Implant Technology, Rostock, Germany) for assistance during biomechanical evaluation of the functional demonstrators, Robert Hauschild and Dirk Pfuetzner (both: FMZ GmbH, Rostock, Germany) for assistance during design development of the functional demonstrator as well as Dr. Melanie Stenzel (TANIOBIS GmbH, Goslar, Germany) for many inspiring discussions.

Conflicts of Interest: J.-O.S., P.H., D.K., J.J., M.-L.S., A.J.-H., and R.B., declare no conflict of interest. A.M. and C.L. are employees of ZM Praezisionsdentaltechnik GmbH, M.W. is an employee of TANIOBIS GmbH, U.L. is an employee of DOT GmbH, and D.R. is an employee of FMZ GmbH.

References

1. Lewis, P.L.; Robertsson, O.; Graves, S.E.; Paxton, E.W.; Prentice, H.A.; W-Dahl, A. Variation and trends in reasons for knee replacement revision: a multi-registry study of revision burden. Acta Orthop. 2021, 92, 182–188, doi:10.1080/17453674.2020.1853340.
2. Goodman, S.B.; Gallo, J. Periprosthetic Osteolysis: Mechanisms, Prevention and Treatment. J. Clin. Med. 2019, 8, doi:10.3390/jcm8122091.

3. Järvenpää, J.; Soininvaara, T.; Kettunen, J.; Miettinen, H.; Kröger, H. Changes in bone mineral density of the distal femur after total knee arthroplasty: a 7-year DEXA follow-up comparing results between obese and nonobese patients. Knee 2014, 21, 232–235, doi:10.1016/j.knee.2013.03.004.
4. Jonitz-Heincke, A.; Sellin, M.-L.; Seyfarth, A.; Peters, K.; Mueller-Hilke, B.; Fiedler, T.; Bader, R.; Klinder, A. Analysis of Cellular Activity Short-Term Exposure to Cobalt and Chromium Ions in Mature Human Osteoblasts. Materials (Basel) 2019, 12, doi:10.3390/ma12172771.
5. Sansone, V.; Pagani, D.; Melato, M. The effects on bone cells of metal ions released from orthopaedic implants. A review. Clin. Cases Miner. Bone Metab. 2013, 10, 34–40, doi:10.11138/ccmbm/2013.10.1.034.
6. Scharf, B.; Clement, C.C.; Zolla, V.; Perino, G.; Yan, B.; Elci, S.G.; Purdue, E.; Goldring, S.; Macaluso, F.; Cobelli, N.; et al. Molecular analysis of chromium and cobalt-related toxicity. Sci. Rep. 2014, 4, 5729, doi:10.1038/srep05729.
7. Crutsen, J.R.W.; Koper, M.C.; Jelsma, J.; Heymans, M.; Heyligers, I.C.; Grimm, B.; Mathijssen, N.M.C.; Schotanus, M.G.M. Prosthetic hip-associated cobalt toxicity: a systematic review of case series and case reports. EFORT Open Rev. 2022, 7, 188–199, doi:10.1530/EOR-21-0098.
8. Glaß, H.; Jonitz-Heincke, A.; Petters, J.; Lukas, J.; Bader, R.; Hermann, A. Corrosion Products from Metallic Implants Induce ROS and Cell Death in Human Motoneurons In Vitro. J. Funct. Biomater. 2023, 14, doi:10.3390/jfb14080392.
9. Lee, D.W.; Du Ro, H.; Han, H.-S.; Lee, M.C. Titanium Alloy Knee Implant Is Associated with Higher Bone Density over Cobalt Chromium: A Prospective Matched-Pair Case-Control Study. Clin. Orthop. Surg. 2023, 15, 581–588, doi:10.4055/cios22082.
10. Bahraminasab, M.; Arab, S.; Doostmohammadi, N. Cytotoxicity and Ion Release of Functionally Graded Al2O3- Ti Orthopedic Biomaterial. JBBBE 2022, 54, 103–118, doi:10.4028/www.scientific.net/JBBBE.54.103.
11. Bahraminasab, M.; Arab, S.; Ghaffari, S. Osteoblastic cell response to Al2O3-Ti composites as bone implant materials. Bioimpacts 2022, 12, 247–259, doi:10.34172/bi.2021.2330.
12. Bahraminasab, M.; Arab, S.; Safari, M.; Talebi, A.; Kavakebian, F.; Doostmohammadi, N. In vivo performance of Al2O3-Ti bone implants in the rat femur. J. Orthop. Surg. Res. 2021, 16, 79, doi:10.1186/s13018-021-02226-7.
13. Bahraminasab, M.; Bozorg, M.; Ghaffari, S.; Kavakebian, F. Electrochemical corrosion of Ti-Al2O3 biocomposites in Ringer's solution. Journal of Alloys and Compounds 2019, 777, 34–43, doi:10.1016/j.jallcom.2018.09.313.
14. Bahraminasab, M.; Ghaffari, S.; Eslami-Shahed, H. Al2O3-Ti functionally graded material prepared by spark plasma sintering for orthopaedic applications. J. Mech. Behav. Biomed. Mater. 2017, 72, 82–89, doi:10.1016/j.jmbbm.2017.04.024.
15. Zhang, Y.; Bandyopadhyay, A. Direct fabrication of compositionally graded Ti-Al2O3 multi-material structures using Laser Engineered Net Shaping. Additive Manufacturing 2018, 21, 104–111, doi:10.1016/j.addma.2018.03.001.
16. Moayedee, Y.; Nikzad, L.; Majidian, H. Exploration into the microstructural, mechanical, and biological characteristics of the functionally graded 3Y-TZP/Ti-6Al-4V system as a potential material for dental implants. J. Mech. Behav. Biomed. Mater. 2024, 151, 106380, doi:10.1016/j.jmbbm.2024.106380.
17. Sun, Q.; Yang, L.; Yang, W.; Ji, H.; Li, M.; Li, Y. Microstructure evolution and bonding mechanism of ZrO2 ceramic and Ti-6Al-4V alloy joints brazed by Bi2O3-B2O3-ZnO glass paste. Journal of the European Ceramic Society 2022, 42, 5953–5963, doi:10.1016/j.jeurceramsoc.2022.06.016.
18. Mick, E.; Tinschert, J.; Mitrovic, A.; Bader, R. A Novel Technique for the Connection of Ceramic and Titanium Implant Components Using Glass Solder Bonding. Materials (Basel) 2015, 8, 4287–4298, doi:10.3390/ma8074287.
19. Bahraminasab, M.; Sahari, B.B.; Edwards, K.L.; Farahmand, F.; Hong, T.S.; Naghibi, H. Material tailoring of the femoral component in a total knee replacement to reduce the problem of aseptic loosening. Materials & Design 2013, 52, 441–451, doi:10.1016/j.matdes.2013.05.066.
20. Vásquez, V.Z.C.; Ozcan, M.; Kimpara, E.T. Evaluation of interface characterization and adhesion of glass ceramics to commercially pure titanium and gold alloy after thermal- and mechanical-loading. Dent. Mater. 2009, 25, 221–231, doi:10.1016/j.dental.2008.07.002.
21. Suansuwan, N.; Swain, M.V. Adhesion of porcelain to titanium and a titanium alloy. J. Dent. 2003, 31, 509–518, doi:10.1016/S0300-5712(03)00071-X.
22. Markhoff, J.; Mick, E.; Mitrovic, A.; Pasold, J.; Wegner, K.; Bader, R. Surface modifications of dental ceramic implants with different glass solder matrices: in vitro analyses with human primary osteoblasts and epithelial cells. Biomed Res. Int. 2014, 2014, 742180, doi:10.1155/2014/742180.
23. Sass, J.-O.; Burmeister, U.; Ganz, C.; Mitrovic, A.; Lang, H.; Bader, R.; Vogel, D. Fracture strength of monolithic and glass-soldered ceramic subcomponents of 5-unit fixed dental prosthesis. J. Prosthodont. 2023, 32, e71-e80, doi:10.1111/jopr.13586.

24. van Vu, T.; Oh, G.-J.; Lim, H.-P.; Yun, K.-D.; Ryu, S.-K.; Yim, E.-K.; Fisher, J.G.; Ban, J.-S.; Park, S.-W. Shear Bond Strength of Zirconia to Titanium Implant Using Glass Bonding. J. Nanosci. Nanotechnol. 2019, 19, 967–969, doi:10.1166/jnn.2019.15913.
25. Farrahnoor, A.; Zuhailawati, H. Review on the mechanical properties and biocompatibility of titanium implant: The role of niobium alloying element. International Journal of Materials Research 2021, 112, 505–513, doi:10.1515/ijmr-2020-8060.
26. Luo, J.P.; Sun, J.F.; Huang, Y.J.; Zhang, J.H.; Zhang, Y.D.; Zhao, D.P.; Yan, M. Low-modulus biomedical Ti-30Nb-5Ta-3Zr additively manufactured by Selective Laser Melting and its biocompatibility. Mater. Sci. Eng. C Mater. Biol. Appl. 2019, 97, 275–284, doi:10.1016/j.msec.2018.11.077.
27. Ozan, S.; Lin, J.; Li, Y.; Wen, C. New Ti-Ta-Zr-Nb alloys with ultrahigh strength for potential orthopedic implant applications. J. Mech. Behav. Biomed. Mater. 2017, 75, 119–127, doi:10.1016/j.jmbbm.2017.07.011.
28. Schulze, C.; Weinmann, M.; Schweigel, C.; Keßler, O.; Bader, R. Mechanical Properties of a Newly Additive Manufactured Implant Material Based on Ti-42Nb. Materials (Basel) 2018, 11, doi:10.3390/ma11010124.
29. Soni, R.; Pande, S.; Salunkhe, S.; Natu, H.; Abouel Nasr, E.; Shanmugam, R.; Hussein, H.M.A.M. In Vitro and Electrochemical Characterization of Laser-Cladded Ti-Nb-Ta Alloy for Biomedical Applications. Crystals 2022, 12, 954, doi:10.3390/cryst12070954.
30. Zhukova, Y.S.; Pustov, Y.A.; Konopatsky, A.S.; Filonov, M.R. Characterization of electrochemical behavior and surface oxide films on superelastic biomedical Ti–Nb–Ta alloy in simulated physiological solutions. Journal of Alloys and Compounds 2014, 586, S535-S538, doi:10.1016/j.jallcom.2013.01.151.
31. Sass, J.-O.; Sellin, M.-L.; Kauertz, E.; Johannsen, J.; Weinmann, M.; Stenzel, M.; Frank, M.; Vogel, D.; Bader, R.; Jonitz-Heincke, A. Advanced Ti–Nb–Ta Alloys for Bone Implants with Improved Functionality. J. Funct. Biomater. 2024, 15, 46, doi:10.3390/jfb15020046.
32. Johannsen, J.; Lauhoff, C.; Stenzel, M.; Schnitter, C.; Niendorf, T.; Weinmann, M. Laser beam powder bed fusion of novel biomedical titanium/niobium/tantalum alloys: Powder synthesis, microstructure evolution and mechanical properties. Materials & Design 2023, 233, 112265, doi:10.1016/j.matdes.2023.112265.
33. Sass, J.-O.; Hembus, J.; Fuhrmann, E.; Vogel, D.; Bauer, E.; Link, H.D.; Bader, R. Pre-clinical characterization of a novel flexible surface stem design for total knee replacements. Proc. Inst. Mech. Eng. H 2023, 237, 1154–1166, doi:10.1177/09544119231197596.
34. Niinomi, M. Mechanical properties of biomedical titanium alloys. Materials Science and Engineering: A 1998, 243, 231–236, doi:10.1016/S0921-5093(97)00806-X.
35. F04 Committee. Test Method for Shear and Bending Fatigue Testing of Calcium Phosphate and Metallic Medical and Composite Calcium Phosphate/Metallic Coatings; ASTM International: West Conshohocken, PA.
36. F04 Committee. Test Method for Shear Testing of Calcium Phosphate Coatings and Metallic Coatings; ASTM International: West Conshohocken, PA.
37. ISO 14243-3:2014-11 Implants for surgery, Wear of total knee-joint prostheses, Part 3: Loading and displacement parameters for wear-testing machines with displacement control and corresponding environmental conditions for test; Beuth Verlag GmbH: Berlin.
38. F02 Committee. Guide for Accelerated Aging of Sterile Barrier Systems for Medical Devices; ASTM International: West Conshohocken, PA.
39. ISO 13179-1:2021 Implants for surgery, Coatings on metallic surgical implants, Part 1: Plasma-sprayed coatings derived from titanium or titanium-6 aluminum-4 vanadium alloy powders; Beuth Verlag GmbH: Berlin.
40. Lochner, K.; Fritsche, A.; Jonitz, A.; Hansmann, D.; Mueller, P.; Mueller-Hilke, B.; Bader, R. The potential role of human osteoblasts for periprosthetic osteolysis following exposure to wear particles. Int. J. Mol. Med. 2011, 28, 1055–1063, doi:10.3892/ijmm.2011.778.
41. Zietz, C.; Reinders, J.; Schwiesau, J.; Paulus, A.; Kretzer, J.P.; Grupp, T.; Utzschneider, S.; Bader, R. Experimental testing of total knee replacements with UHMW-PE inserts: impact of severe wear test conditions. J. Mater. Sci. Mater. Med. 2015, 26, 134, doi:10.1007/s10856-015-5470-y.
42. Vercaigne, S.; Wolke, J.G.; Naert, I.; Jansen, J.A. Histomorphometrical and mechanical evaluation of titanium plasma-spray-coated implants placed in the cortical bone of goats. J. Biomed. Mater. Res. 1998, 41, 41–48, doi:10.1002/(sici)1097-4636(199807)41:1<41:aid-jbm5>3.0.co;2-q.
43. Ozeki, K.; Yuhta, T.; Aoki, H.; Nishimura, I.; Fukui, Y. Push-out strength of hydroxyapatite coated by sputtering technique in bone. Biomed. Mater. Eng. 2001, 11, 63–68.
44. Müller, M.; Hennig, F.F.; Hothorn, T.; Stangl, R. Bone-implant interface shear modulus and ultimate stress in a transcortical rabbit model of open-pore Ti-6Al-4V implants. J. Biomech. 2006, 39, 2123–2132, doi:10.1016/j.jbiomech.2005.05.036.
45. Li, J.; Liao, H.; Fartash, B.; Hermansson, L.; Johnsson, T. Surface-dimpled commercially pure titanium implant and bone ingrowth. Biomaterials 1997, 18, 691–696, doi:10.1016/s0142-9612(96)00185-8.

46. Chang, C.K.; Wu, J.S.; Mao, D.L.; Ding, C.X. Mechanical and histological evaluations of hydroxyapatite-coated and noncoated Ti-6Al-4V implants in tibia bone. J. Biomed. Mater. Res. 2001, 56, 17–23, doi:10.1002/1097-4636(200107)56:1<17:aid-jbm1063>3.0.co;2-t.
47. Zelle, J.; Janssen, D.; Peeters, S.; Brouwer, C.; Verdonschot, N. Mixed-mode failure strength of implant-cement interface specimens with varying surface roughness. J. Biomech. 2011, 44, 780–783, doi:10.1016/j.jbiomech.2010.10.037.
48. Hey, J.; Kasaliyska, M.; Kiesow, A.; Schweyen, R.; Arnold, C. Retentive Force of Glass-Ceramic Soldered Customized Zirconia Abutment Copings with Prefabricated Titanium Bases. Materials (Basel) 2020, 13, doi:10.3390/ma13143193.
49. Travessa, D.; Ferrante, M. The Al2O3-titanium adhesion in the view of the diffusion bonding process. Journal of Materials Science 2002, 37, 4385–4390, doi:10.1023/A:1020669022776.
50. Gibbesch, B.; Elssner, G.; Petzow, G. Microstructure of interface regions and mechanical properties of Ti/Al 2O 3 and Ti-alloy/Al 2O 3 joints for dental implants. Clin. Mater. 1990, 5, 177–189, doi:10.1016/0267-6605(90)90017-P.
51. Gibbesch, B.; Elssner, G.; Petzow, G. Investigation of Ti/Al2O3 joints with intermediate tantalum and niobium layers. Biomaterials 1992, 13, 455–461, doi:10.1016/0142-9612(92)90166-L.
52. Rahaman, M.N.; Huang, T.; Bal, B.S.; Li, Y. In vitro testing of Al(2)O(3)-Nb composite for femoral head applications in total hip arthroplasty. Acta Biomater. 2010, 6, 708–714, doi:10.1016/j.actbio.2009.07.025.
53. Bergmann, G.; Bender, A.; Graichen, F.; Dymke, J.; Rohlmann, A.; Trepczynski, A.; Heller, M.O.; Kutzner, I. Standardized loads acting in knee implants. PLoS One 2014, 9, e86035, doi:10.1371/journal.pone.0086035.
54. Dreyer, M.J.; Trepczynski, A.; Hosseini Nasab, S.H.; Kutzner, I.; Schütz, P.; Weisse, B.; Dymke, J.; Postolka, B.; Moewis, P.; Bergmann, G.; et al. European Society of Biomechanics S.M. Perren Award 2022: Standardized tibio-femoral implant loads and kinematics. J. Biomech. 2022, 141, 111171, doi:10.1016/j.jbiomech.2022.111171.
55. Sass, J.-O.; Jakobi, A.; Mitrovic, A.; Ganz, C.; Wilken, J.; Burmeister, U.; Lang, H.; Bader, R.; Vogel, D. Bending strength of ceramic compounds bonded with silicate-based glass solder. Materials Testing 2021, 63, 593–598, doi:10.1515/mt-2020-0098.